Chapter 7

Recent Advances in TiO_2 Nanotube-Based Materials for Photocatalytic Applications Designed by Anodic Oxidation

Phuoc Huu Le and Jihperng Leu

Additional information is available at the end of the chapter

http://dx.doi.org/10.5772/intechopen.77063

Abstract

This book chapter reports some spectacular and interesting 1D nanostructures of TiO_2, which are grown by the anodic oxidation. Under suitable conditions, conventional one-step anodic oxidation is available to grow TiO_2 nanotube arrays (TNAs) and TiO_2 nanowires/nanotubes; meanwhile, two-step anodic oxidation allows fabricating some novel TNAs with spectacular morphologies such as highly ordered TNAs, bamboo-type TNAs, and lotus root-shaped TNAs. The formation mechanisms of these nanostructures during the anodic oxidation processes are elusive via studying effects of several key parameters such as oxidizing voltage, processing time, and electrolytes. In addition, the photocatalytic activity of the TNA-based nanomaterials is characterized by the degradation of pharmaceutical model, methylene blue, or the photoelectrochemical effect.

Keywords: TiO_2 nanotube arrays, anodic oxidation, formation mechanism, photocatalysts, PEC

1. Introduction

Titanium dioxide (TiO_2) is the most widely used one for applications in photocatalysis, dye-sensitized solar cells, and biomedical devices owing to some outstanding properties [1–8]. The fascinating properties like strong oxidizing abilities, chemical stability, nontoxicity, ease of preparation, favorable band-edge positions, water insolubility, multifaceted electronic properties, and super hydrophilicity. TiO_2 has three metastable phases of rutile, brookite, and anatase, in which rutile (E_g = 3.0 eV) and anatase (E_g = 3.2 eV) are the most commonly synthesized

and used phases for applications. Rutile is the most stable phase for bulk TiO_2, while it is anatase phase for nanoscale size crystallite TiO_2 due to surface energy effect [9]. Anatase can transfer into rutile by annealing temperatures in range of 500–700°C. Compared to rutile phase of TiO_2, anatase generally possesses better photocatalytic activity owing to its wider bandgap (~3.2 eV), lower electron–hole recombination rate, and higher charge carrier mobility.

For many applications of TiO_2, it is crucial to maximize the specific surface area to enhance catalytic reactions and achieve a maximum overall efficiency. Therefore, nanoparticulated forms of TiO_2 are widely used [1]. Though providing high surface area, the charge carrier transport of nanoparticulated forms is limited due to the structural disorders. Instead, 1D TiO_2 nanostructures such as TiO_2 nanotube arrays (TNAs) and TiO_2 nanowires on nanotube arrays (NTWs/TNAs) are of great interests because of the higher control of the chemical or physical behavior. By diminishing dimensions to the nanoscale, TNAs and TNWs/TNAs not only provide large surface-to-volume ratio and unidirectional electrical channel but also may change the electronic properties owing to quantum size effects' strong contribution of surface reconstruction or surface curvature. Complex hybrid nanostructures such as TNWs/TNAs [10], brush-type nanostructure [11], and bamboo-type TiO_2 nanotube [12] have been fabricated successfully by anodic oxidation, which have a great potential to simultaneously provide high surface area, good charge transport, and usually have better performance than simple nanostructures. It is worthy to mention that the form of nanostructured TiO_2 film on Ti substrate offers a great advantage that it is able to retrieve after usage in photocatalytic applications. TiO_2 nanotubes were readily fabricated by template-assisted processes, hydrothermal method, and electrochemical anodic oxidation [1, 3, 6, 13]. Among these methods, TNAs prepared by electrochemical anodization are simple, cost-effective, recyclable, suitable for rapid production, and notable to yield uniform TNAs with vertical alignment and diverse morphology [1, 6, 10, 14, 15].

This book chapter provides some of the spectacular and surprising 1D nanostructures of TiO_2 prepared by anodic oxidation method for photocatalytic applications. The first section will focus exclusively on the growths of self-organized TNAs and TNWs/TNAs using conventional one-step anodic oxidation as well as their photocatalytic performances. The second section will review some novel modified TNA structures fabricated by two-step anodic oxidation, including highly ordered TNAs, the modified TNAs, and their photoelectrochemical water splitting performance.

2. One-dimensional nanostructured TiO_2 grown by one-step anodic oxidation

2.1. TiO_2 nanotube arrays (TNAs): formation mechanism and photocatalytic activity

In 1999, Zwilling and coworkers reported the first self-organized anodic oxides on titanium in chromic acid electrolytes containing hydrofluoric acid [16]. In this work, an organized nanotube layer with thickness up to approximately 500 nm was grown on a Ti sheet at low voltage.

http://dx.doi.org/10.5772/intechopen.77063

However, the tube structure was not highly organized, and the tubes showed considerable sidewall inhomogeneity [16]. Moreover, the thickness of TNA layer did not increase with anodizing time, and the limited thickness was ascribed to an oxide growth/chemical dissolution equilibrium (steady state).

Figure 1 illustrates the setup of an anodic anodization process in our experiments that is also a typical process in the literature. Titanium foils (99.9% purity, 0.5 mm thickness) are used as the substrate for growing 1D nanostructures of TiO_2. Prior to anodization, Ti foil was ultrasonically cleaned in acetone, methanol, and deionized water (each solvent 10 min) and then dried by a purging N_2 gas. The TNA film area on Ti foil is 1 × 1.5 cm. The anodization is carried out at room temperature using a two-electrode system with the Ti foil as an anode and a stainless steel foil (SS304 or platinum plate for researches) as a cathode. The electrolytes consisted of 0.5 wt% NH_4F in solution of ethylene glycol and water (99:1 in wt.%). The applied voltage of 30–60 V and anodizing time of 0.5–6 hrs are usually used.

2.1.1. Formation mechanism of TiO_2 nanotubes

TNA growth is driven by two simultaneously occurring reactions in the anodization process: (1) the electric field-driven anodic oxidation of Ti to form TiO_2 and (2) the electric field-assisted chemical dissolution of the TiO_2 layer [8, 14]. The reactions are given below:

$$\text{Anodic reaction: } Ti + 2H_2O – 4e = TiO_2 + 4H^+ \quad (1)$$

$$\text{Cathodic reaction: } 4H^+ + 4e = 2H_2 \quad (2)$$

$$\text{Chemical etching (dissolution) reaction: } TiO_2 + 6F^- + 4NH_4^+ = TiF_6^{2-} + 2H_2O \quad (3)$$

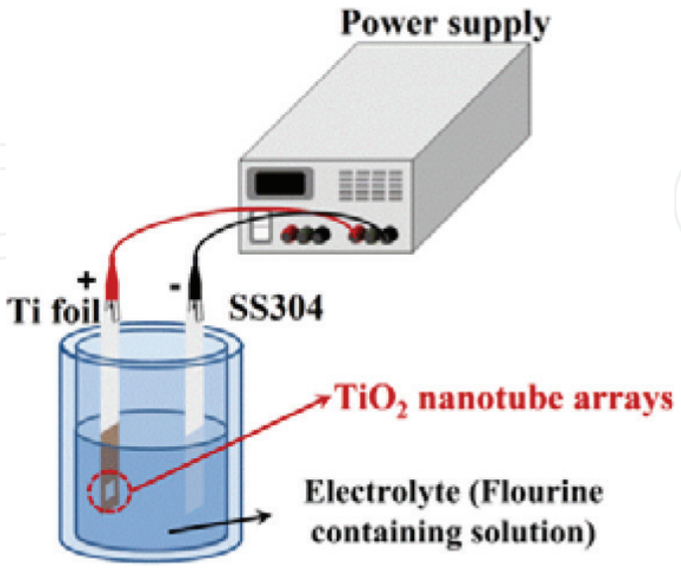

Figure 1. A schematic of an electrochemical anodization process.

In the anodic oxidation process, the current density (j) changes with anodizing time (t). **Figure 2(a)** illustrates the current transient curve recorded during the anodization of titanium foil. Initially, the current density rapidly decreases, then slightly increases, and finally remains a constant [1]. According to the variations of current density with reaction time, three stages of the TNA growth process were defined as shown in **Figure 2(a)**. In the early stages (I), the current density rapidly decreases because of the formation of the non-conductive thin oxide layer (see also **Figure 2(b)**). Next, there is a slight increase in the current density owing to the local growth of pits. Finally, the current density remains a constant due to reaching the balance between field-assisted anodic oxidation and chemical–/field-assisted dissolution current, and the initial pits will grow and develop into nanotube arrays. Notably, the diameter and length of the nanotubes gradually increase when the dissolution rate of the wall of the nanopores is slower than that of the growth rate of nanopores. And, the diameter and length of NTs no longer change when the growth rate is equal to the dissolution rate [17].

2.1.2. An application of TiO_2 nanotubes in photoelectrocatalytic degradation of model environmental pharmaceuticals

A selected optimal TiO_2 nanotube was prepared at 30 V for 16 h in ethylene glycol solution containing 0.20 mol L^{-1} NH_4F and 0.50 mol L^{-1} HAc. **Figure 3(a)** shows structure-morphology of the TNAs through the FESEM and HRTEM images. Clearly, perfect NTAs are obtained with average inner diameter approximately 70 nm length of about 7.5 μm. TNAs have anatase phase which is confirmed by the selected area electron diffraction pattern recorded from the circled area. In addition, the lattice fringes spacing of 0.352 nm corresponds to {101} planes of anatase TiO_2. To evaluate the photocatalytic activity of the TNA photoanodes, the authors

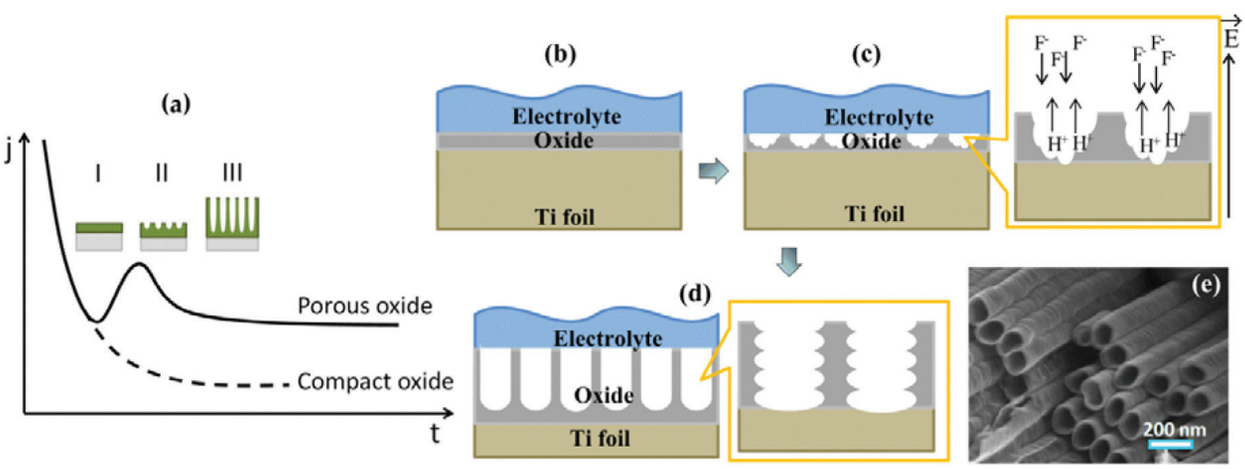

Figure 2. (a) Typical current–time (*j–t*) characteristics after applied voltage in the absence (**---**) and presence (—) of fluoride ions in the electrolyte. Either compact oxide (fluoride free) or porous/tubular metal oxide formation (containing fluoride) formed by different morphological stages (I–III). The growth process of TiO_2 nanotube arrays (TNAs): (b) non-conductive thin oxide layer forming, (c) local growth of the pits, and (d) growth of the semicircle pores and developed nanotube arrays. (e) a typical TNA prepared by using an electrolyte consisting of ethylene glycol and water (99:1 in wt%) with 0.5 wt% NH_4F, at 30 V for 30 mins.

http://dx.doi.org/10.5772/intechopen.77063

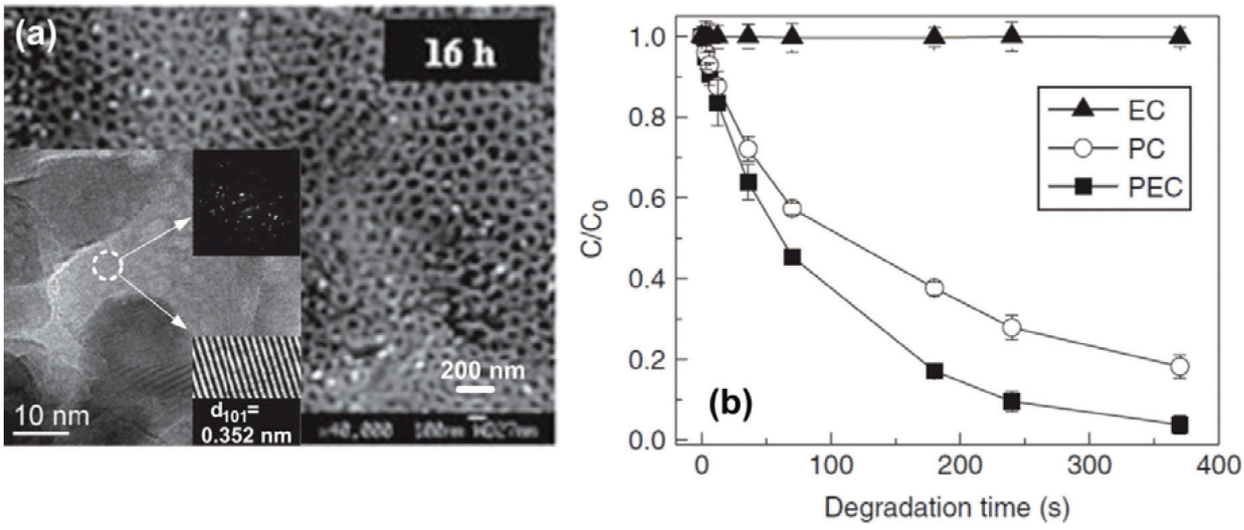

Figure 3. TiO_2 nanotubes prepared at 30 V for 16 h in ethylene glycol solution containing 0.50 Mol L^{-1} HAc and 0.20 Mol L^{-1} NH_4F: (a) FESEM image and a HRTEM image of nanotube wall (inset), (b) degradation of acyclovir under different processes including electrolysis (EC), photocatalysis (PC), and photoelectrocatalysis (PEC) using the TiO_2 nanotube photoanode [17].

performed experiments using a model compound of pharmaceutical, acyclovir (20 mg L^{-1}), in a three-electrode thin layer photoelectrochemical reactor with a reaction volume of 100 μL under UVA irradiation [17]. An aqueous solution containing 0.2 mol $-^{1}$ $NaNO_3$ and 20 mgL^{-1} acyclovir was injected into the reactor under different constant speeds to adjust the reaction time. An applied potential of +1 V constant and illumination of 10 mWcm^{-2} from UV-LED array were used for the PEC experiment. Photocatalysis (PC) and electrolysis (EC) degradation experiments were conducted under identical experimental conditions as photoelectrocatalysis (PEC) experiments, except the electrochemical system was disconnected and the light switched off, respectively [17].

Figure 3(b) presents the degradation of acyclovir under EC, PC, and PEC processes using the TNA photoanode. There was no measurable change in acyclovir concentration within residence time up to 370 s for the EC process. The degradation efficiencies of acyclovir in the PC process were 62.0 and 69.0% at residence times of 180 and 370 s, respectively. In comparison, the PEC degradation efficiencies increased remarkably to 83.0% at 180 s and 96.2% at 370 s. The significantly faster degradation of acyclovir for PEC process than those of PC and EC is attributed to two reasons: First, under an appropriate applied potential bias to the photoanode, it is enable to remove the photogenerated electrons and prolong the lifetime of photoholes for direct photohole reactions, and the oxidation power of the photoholes (3.1 V) is greater than that of photogenerated radicals such •OH (2.8 V) [17]. Second, the light adsorption capability and charge transfer is enhanced owing to the tubular structure of the TNA photoanode. Thus, the separation of photogenerated electrons and holes assisted by the application of a potential bias is accelerated, which in turn enhances the concentration of photoholes and promotes effectively the degradation of acyclovir.

2.2. TiO_2 nanowires on nanotube arrays (TNWs/TNAs)

2.2.1. Fabrication of TiO_2 films and other experimental details

TiO_2 films with morphology of TNWs/TNAs were grown on Ti foils by anodic oxidation. The electrolyte consists of ethylene glycol and water (99:1 in wt%) and 0.5 wt% NH_4F. First, the anodizing voltage was varied from 20 to 80 V at a fixed processing time of 1 h. Then, the anodizing time varied from 30 to 120 min at a fixed voltage of 40 V. After fabrication of the TNWs/TNAs, thermal annealing was performed in the air at 450°C for 2 h, at a heating rate of 2°C/min.

2.2.2. Effect of anodization voltage

Figure 4 shows the surface morphology of the TiO_2 films prepared at different anodizing voltages from 20 to 80 V, in a 0.5 wt% NH_4F solution, and at a constant anodizing time of 1 h. At 20 V, it exhibits highly ordered TNAs with a tube inner wall diameter of 40 nm and a wall thickness of 20 nm. Meanwhile, as increasing the voltage to 40 V, TNWs with a wire width ~50 nm appears on the top of TNAs which has tube diameters of 60 nm in diameter and ~10 nm in wall thickness. When the voltage increases to 60 V, TNWs with a width of ~20 nm fully covered on the TNAs with a tube diameter of 80 nm and a wall thickness of ~10 nm. Strikingly, TNW-free TNAs with a tube diameter of ~110 nm are obtained at a high voltage of 80 V [10].

2.2.3. Effect of anodization time

In order to explore the formation mechanism of TNWs/TNAs, we observe the morphology evolution of TiO_2 film as a function of anodizing time from 30 to 120 min at a fixed anodizing voltage of 40 V (**Figure 5**). At 30 min, a highly ordered TNA structure is obtained, and it has a tube length of 12.2 μm, diameter of 60 nm, and wall thickness of 18 nm. The steady-state growth rate of the TNA length at up to 30 min is ~0.4 μm/min. As further increasing the anodizing time to 35, 38, and 40 min, the surface morphology near the top of the TNA exhibits a gradual change. Indeed, the wall thickness decreases from 18 nm at 30 min to 12 nm at 35 min near the top of the TNAs due to the increased electrochemical etching with anodizing time. Noticeably, the wall thickness of the 35-min TNAs almost remains the same value of ~18 nm in the middle section of nanotubes (see the inset), implying that enhanced electrochemical etching occurs near the top of the nanotube mouths, with respect to the middle section. It is a transitional stage at 38 and 40 min, where the wall thicknesses are even thinner and especially the tubes start disintegrating. After 45 min, TNAs near the top surface are broken up, along with thinning of wall thickness down to ~10 nm. At 60 min, TNWs with a width of ~50 nm is covered on surface. The nanowires fell down on the top of the TNAs as its length is over ~2 μm. At longer anodizing time of 90 and 120 min, TNWs are completely covered on the top of TNAs. Due to chemical etching, the width of TNWs decreased from 50 nm (at 60 min) down to ~30 nm (at 90 min) and then to ~20 nm (at 120 min). Moreover, as the time increase from 90 to 120 min, the nanowire structure emerges upon further etching, while the length of the TNAs is slightly increased from 11 μm (90 min) to 12 μm (120 min) [10].

http://dx.doi.org/10.5772/intechopen.77063

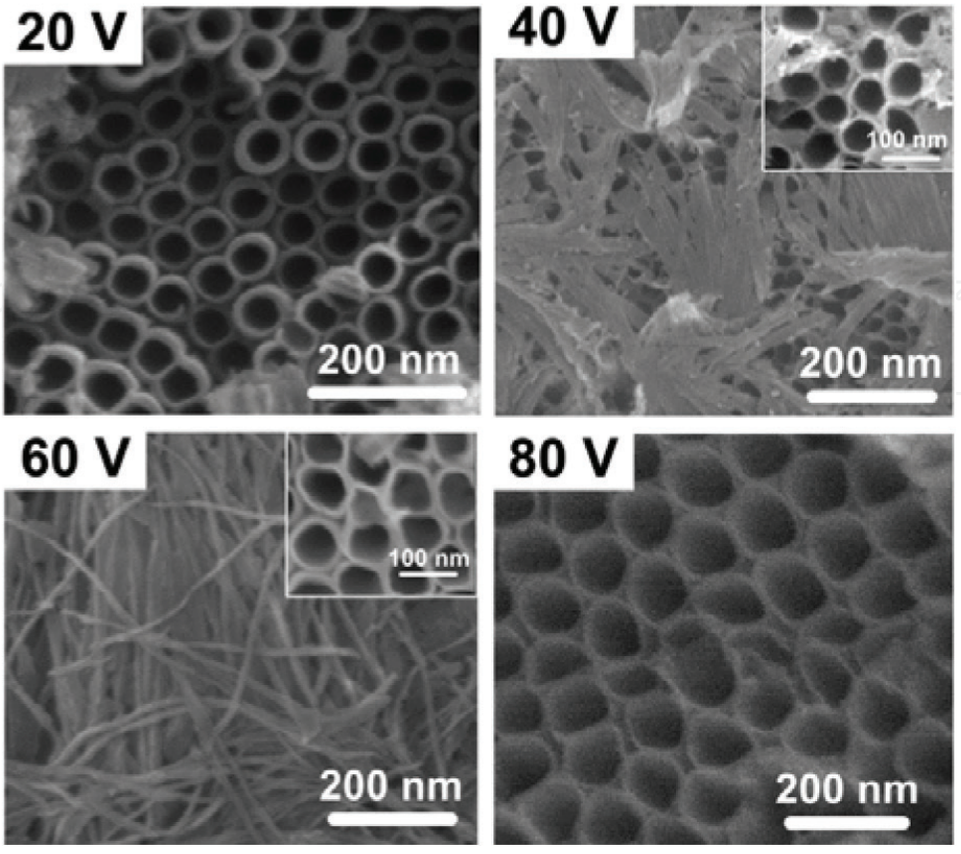

Figure 4. Anodizing voltage dependence of surface morphology for the TiO_2 films prepared by anodic oxidation at a constant anodizing time of 1 h [10].

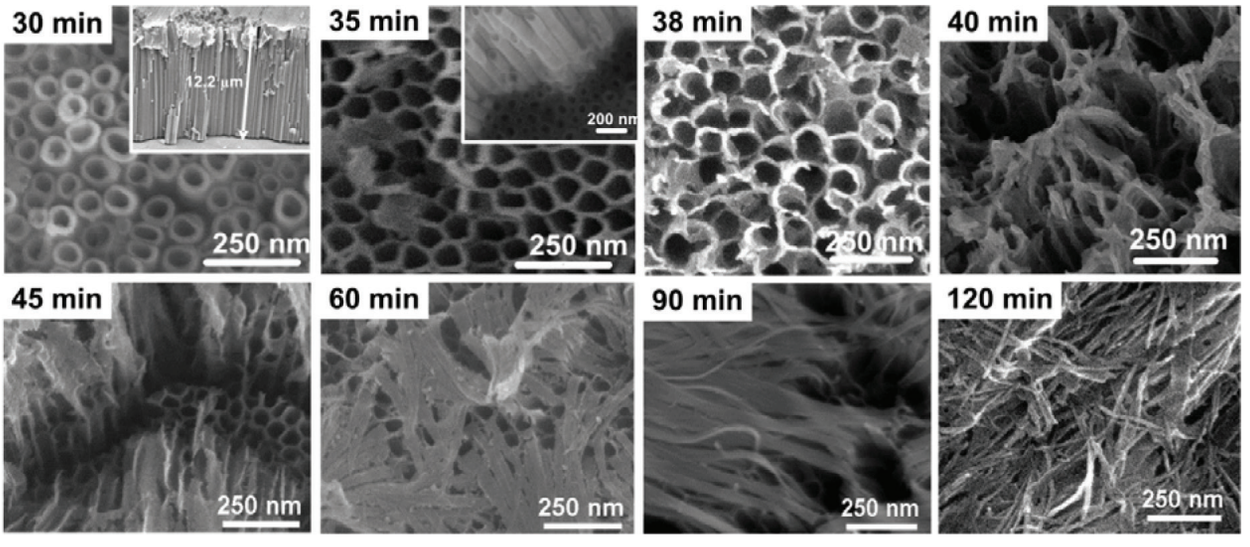

Figure 5. Anodizing time dependence of surface morphology of the TiO_2 films prepared by anodic oxidation under at a constant anodizing voltage of 40 V [10].

The formation of TNWs/TNAs is governed by two key factors of (1) the strength of the electric field and (2) the processing time. In fact, **Figure 6(a)** summarizes the required conditions for forming TNWs/TNAs as functions of anodizing voltage and processing time in a fixed

electrolyte solution. For example, TNWs/TNAs are obtained for 120 min at 30 V; meanwhile, it takes only 30 min for anodizing voltage of 50–60 V. The influence of the electric field strength on the formation of TNWs/TNAs is elucidated by considering the ion migration under electric field in the electrolyte. In principle, the flux of ions in the presence of electric field can be expressed as [10]

$$J_i = -D_i \frac{\partial c_i}{\partial x} - u_i c_i E \tag{4}$$

where J_i is the flux of species i of concentration c_i in direction x, D_i is the diffusion coefficient, $\partial c_i/\partial x$ is the concentration gradient, u_i is the mobility of species i, and E is the electric field strength. Evidently, since ion migration in the electric field is considerable to the ion diffusion process under a concentration gradient, the field strength significantly drives the ion transport in the electrolyte. According to Eq. 4, higher field strength leads to higher ion flux in the electrolyte. Consequently, under a high field strength (or high voltage), the TNW/TNA structure is formed in a shorter time. Notably, the growth of TNWs with characteristic of longer processing times for lower voltages is only found in the anodizing voltage range of 30–60 V. To get a deeper insight into the role of electric field strength in the formation of TNWs onto TNAs, the voltage dependence of the pore diameter and wall thickness of TNA's top section before the emergence of nanowires is investigated, and the results are shown in **Figure 6(b)**. For the cases with no TNW formation, for example, at ≤20 or ≥ 80 V, the tube diameter and wall thickness are obtained from TNAs prepared at anodizing time of 30 min. As can be seen in **Figure 6(b)**, the pore diameter of the TNA's mouth increases from 30 to 110 nm with increasing the voltage from 10 to 80 V, agreeing with the reported results [18]. Meanwhile, the wall thickness of the TNA's mouths decreases from 20 to 8 nm when the applied voltage is increased from 10 to 80 V. The TNW/TNA film is only found when the tube wall thickness is in range of 10–15 nm. As shown in **Figure 6(a)** and **(b)**, the dissolution rate would be too low to break up TiO_2 tube wall when the applied voltage is sufficiently low and thus only TNA structure is found. By contrary, if the anodizing voltage is too high, which

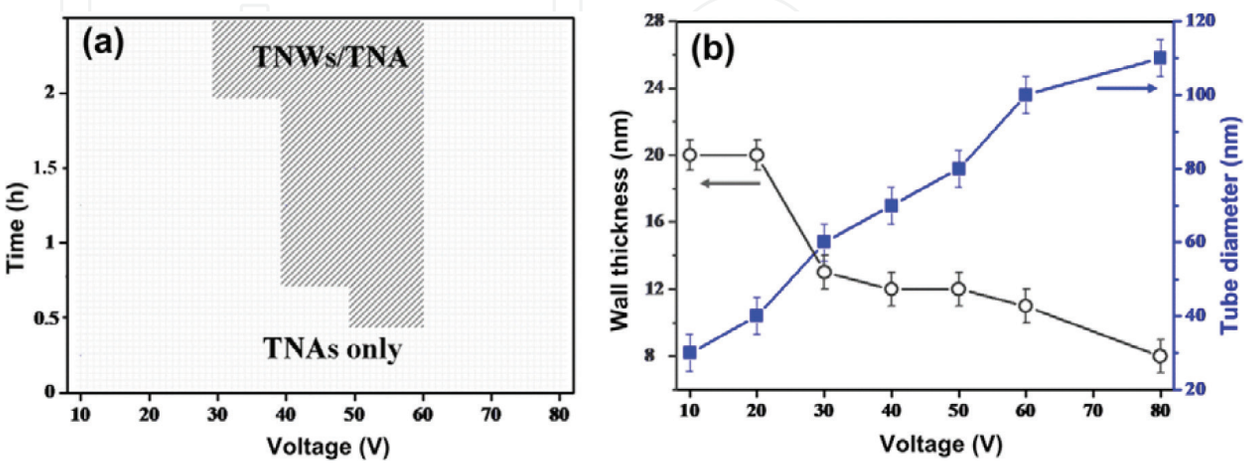

Figure 6. (a) Conditions of required anodizing voltage and processing time (shaded zone) for forming TNWs/TNAs. (b) The pore diameter and wall thickness of TNA's top section prior to the emergence of nanowires, as a function of voltage.

http://dx.doi.org/10.5772/intechopen.77063

leads to high dissolution rate to completely remove the top section of TiO_2 nanotubes, and consequently TNW-free TNAs with a thin wall thickness of ~8 nm are observed.

2.2.4. Formation mechanism of TNWs/TNAs

At some proper conditions of anodic oxidation, TNW's cover on TNAs can be fabricated. J. H. Lim et al. proposed the "bamboo-splitting" model for the TNW formation mechanism [19]. In addition, the formation TNWs can also be clearly explained "strings of through holes" model by M.Y. Hsu et al., as illustrated in **Figure 7** [10]. It follows four stages. First, the ordered TNAs are formed as processing the anodization, accompanying with field-enhanced chemical drilling by a high H^+ concentration at the pore bottom of nanotubes, in conjunction with a protective environment maintained along the pore walls by the highly viscous EG solution. At this stage, field-enhanced further dissolution in the tube bottom is still occurring during anodization process (**Figure 7(a)**). Second, the migration of F^- ions toward the electric field to the bottom of anode is inhibited by the highly viscous solution, which results in the much higher F^- concentration at the tube than at the tube bottom. Notably, in the electrolyte with water content, the chemical dissolution reaction of TNAs is further enhanced by hydrogen ions (reaction (3) above). Consequently, the tube mouth part is thinner than the lower sections, as shown in **Figure 7(a)**. The inner tube is found to be nonuniform and rough (**Figure 7(b)** inset), and thus when the tube mouth is thin enough

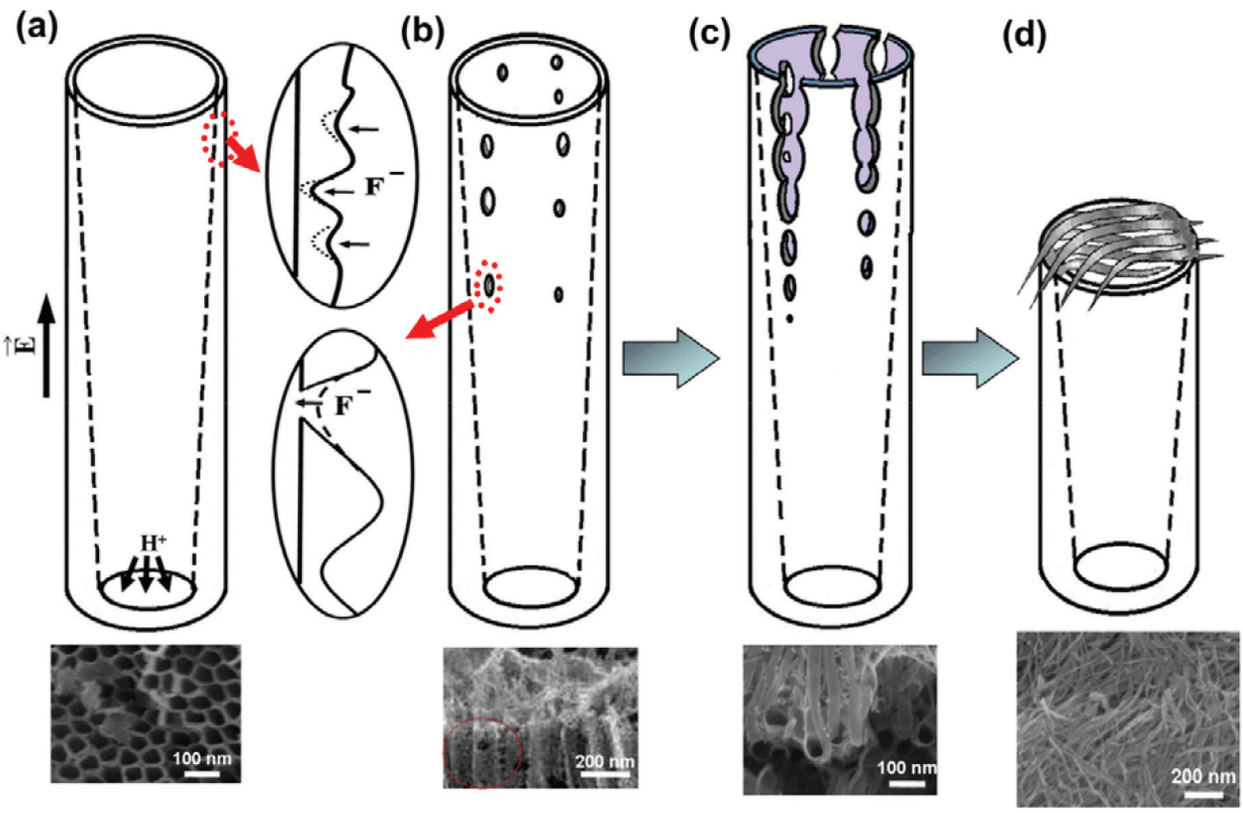

Figure 7. Schematic diagrams and corresponding SEM images of four stages in the TNW/TNA formation mechanism: (a) thinning the tube wall thickness with high roughness near the TNA's mouths, (b) forming strings through holes in the top section of TNAs, (c) splitting into nanowires, and (d) collapsing and further thinning of nanowires [10].

(< 10 nm), it can be etched through under high dissolution reaction with high concentration of F^- ions (**Figure 7(b)**). By increasing processing time, strings of through holes are formed on the tube wall, and they would initiate and propagate downward from the top to bottom of TNAs (or along the F^- migration direction), while the holes near the top expand and connect to split into nanowires (**Figure 7(c)**) as the anodizing time increases. With further increasing anodizing time, the nanowires exhibit smooth at the edges and narrower wire width due to the sufficient chemical etching. When the wire length is too long (i.e., over ~5 μm), the nanowires would collapse onto TNAs, as illustrated in **Figure 7d**. Briefly, the proposed formation mechanism of TNWs/TNAs by one-step anodic oxidation follows four stages: (a) thinning the tube wall thickness with high roughness near the TNA's mouths, (b) forming strings through holes in the top section of the TNAs, (c) splitting into nanowires, and (d) collapsing and further thinning of nanowires [10].

2.2.5. Photocatalytic performance

The photocatalytic performance of TNW/TNA nanostructure in comparison with other morphologies of TNAs and TiO_2 nanoparticles is presented in this part. The TiO_2 P25 nanoparticle films were fabricated by the doctor-blade method. For making a reliable comparison, the film thickness of TiO_2 nanoparticles was controlled to be comparable to that of TNW/TNA films (~11 μm) by controlling the height of the blade above the Ti substrate and/or the concentration of TiO_2 paste. The effect of various TiO_2 morphologies on the photocatalytic degradation of methylene blue (MB) was examined under the 360 nm wavelength irradiation of an 8 W HeCd lamp. To make a reliable comparison, diameters of nanotubes (40–100 nm)

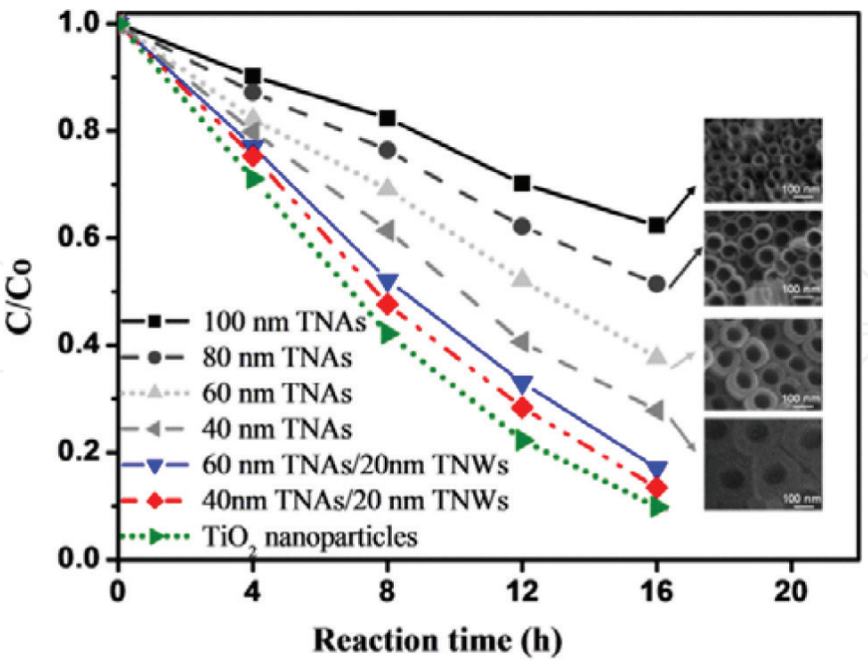

Figure 8. Photocatalytic degradation of methylene blue of various TNAs, TNWs/TNAs, and TiO_2 nanoparticle films, C/C_0 vs. reaction time under UV light irradiation (8 W, 360 nm wavelength) [10].

http://dx.doi.org/10.5772/intechopen.77063

and film thickness (~11 μm) are kept almost the same between TNAs and TNWs/TNAs by adjusting processing conditions. **Figure 8** shows the photocatalytic activity of TNAs and TNW/TNA films and TiO_2, C_t/C_0 as a function of UV irradiation time, in a MB solution with $C_0 = 2.5 \times 10^{-5}$ M. We used the pseudo first-order kinetics as described by the Langmuir-Hinshelwood model [20]. Thus, the photodegradation rate of MB could be expressed by the following Eqs. (5) and (6):

$$C_t = C_o e^{-kt} \tag{5}$$

$$\ln C_t/C_o = -kt \tag{6}$$

where k is the reaction rate constant, t is the irradiation time, and C_0 and C_t are the initial concentration and the reaction concentration of MB. The reaction rate constants (k) were calculated from the experimental data using a linear regression. For TNAs with various tube diameters at a fixed tube thickness, the k values were 9.80×10^{-2}, 8.48×10^{-2}, 6.73×10^{-2}, and 5.49×10^{-2} h^{-1} for tube diameter of 40, 60, 80, and 100 nm, respectively. Clearly, a smaller tube diameter results in a higher reaction rate [10]. In comparison, at the same tube diameter of 60 nm, the k value of 20 nmTNWs/60 nmTNAs was 48% higher than that of pure TNAs (12.54×10^{-2} vs. 8.40×10^{-2} h^{-1}). Similarly, at a fixed tube diameter of 40 nm, the rate constant k for 20 nm TNWs/40 nm TNAs enhanced approximately 33% over the pure TNA one (13.05×10^{-2} vs. $\times 9.8 \times 10^{-2}$ h^{-1}) [10]. It is found that the photocatalytic activity of TNWs/TNAs enhanced remarkably (up to 33–48%) over the corresponding pure TNAs.

Table 1 summarizes the calculated dye adsorption and the k values of various TiO_2 films. For TNAs, a smaller tube diameter yields a higher dye adsorption because of its larger surface area, which results in enhanced photocatalytic efficiency. The difference in surface area of TNAs comes from different densities of nanotube. As the anodizing voltage increases, tube density decreases with increasing tube diameter to result in a decrease of dye adsorption and photocatalytic efficiency. The dye adsorption of TNWs/TNAs is significantly higher than that of the corresponding TNA film because the former that offers larger surface area than the latter. Indeed, the congregation of the bundled nanowires connected to the nanotube mouths induces surface area enhancement over the TNAs. It is also found from **Table 1** that the change percentages of the reaction rate constants for both TNAs and TNWs/TNAs are higher than those of dye adsorption. This indicates that besides the predominant factor of surface area, the 1D nanostructures of TNAs and TNWs/TNAs offer the promotion of charge transport and reduced recombination rate. Though having smaller surface area than TiO_2 nanoparticles, both the faster transport and slower recombination of 1D structures and the providing additional surface area from TNWs, the photocatalytic performance of TNWs/TNAs has achieved a very high efficiency ($k = 13.05 \times 10^{-2}$ h^{-1}) that is very close to the k value of TiO_2 nanoparticles (13.05×10^{-2} h^{-1}) [10]. It is worthy to mention that the immobilized film forms (i.e., TNAs and TNWs/TNAs on Ti plates) are more practical than TiO_2 powdery form. The photocatalytic performance of TNWs/TNAs may be further improved by optimizing the width and density of TNWs covering on TNAs.

TiO_2 film	Dye adsorption ($\times 10^{-8}$ mol/cm^2)	Change (%) relative to nanoparticles	Reaction rate constants (k ($\times 10^{-2}$ h^{-1}))	Change (%) relative to nanoparticles
100 nm TNAs	1.22	29%	5.49	38%
80 nm TNAs	1.65	39%	6.73	47%
60 nm TNAs	2.33	55%	8.48	59%
40 nm TNAs	2.72	64%	9.80	68%
60 nm TNAs/20 nm TNWs	3.21	76%	12.54	87%
40 nm TNAs/20 nm TNWs	3.58	85%	13.05	91%
TiO_2 nanoparticles	4.22	100%	14.38	100%

Table 1. Dye adsorption, reaction rate constants (k), and change percentage of various TiO_2 films.

3. Highly ordered TNAs and modified TNAs designed by two-step anodic oxidation

Using one-step anodization, the produced TNAs usually present disparity in tube lengths and relatively rough surfaces. It has been recently demonstrated that a two-step anodization is possible for preparation of highly ordered and uniform TNAs [14, 15] or unique hierarchical top layer/TNAs with significantly better performances in dye-sensitized solar cells [21] and in photoelectrochemical (PEC) water splitting [6]. A typical process of two-step anodization includes (1) the one-step anodization for growth TiO_2 nanotubes, (2) subsequent removal of the as-grown TNAs by ultrasonication, and (3) the two-step anodization to grow TiO_2 NTs from the same substrate [14, 15].

3.1. Highly ordered TNAs

The SEM images of the highly ordered nanotubes, bamboo-type nanotubes, and lotus root-shaped nanostructure of TiO_2 are shown in **Figure 9**. These nanostructures are prepared by two-step anodization method, in which electrolyte contained ethylene glycol ($C_2H_6O_2$), 0.25% (in mass) NH_4F and 1% (in volume) H_2O. Noticeably, prior to performing the anodization, the electrolyte was aged under a voltage of 60 V for 60 h. In the first step, a Ti foil was anodized at 60 V for 24 h to grow a layer of TiO_2 nanotubes, and then the layer was removed ultrasonically in deionized water. **Figure 9(a)** and **(c)** shows the top view and side view of the TNAs prepared under an anodizing voltage of 60 V in the two-step anodization, which is much more uniform in alignment and length than the TNAs fabricated by the corresponding one-step anodization [15]. **Figure 9b** presents the imprint pattern left on the Ti surface after peeling off from the Ti foil ultrasonically. Clearly, each nanotube is surrounded by six nearest neighbors, and each nanotube has six protrusions with hexagonal

http://dx.doi.org/10.5772/intechopen.77063

pattern at the fringe of its top end, suggesting that the nanotubes in the two-step anodization directly developed from the imprint pattern left on the Ti surface. It is found that the aging the electrolyte is necessary for improving the quality of the imprint patterns or avoiding the initial random patterns of TNAs. The ordered imprints play the role of template for the nanotube growth. Owing to the regular distribution across the surface of the pretreated Ti foil at the very beginning, the uniformity and orderliness of the nanotube arrays were developed during the two-step anodization [15]. Intriguingly, a thin porous film is covered on the top of the nanotube layer as taking a closer look at **Figure 9a**. It is well known that the length of a nanotube does not increase when the rate of oxidation at the Ti/oxide interface at the bottom equals the rate of dissolution at the oxide/electrolyte interface at the top. Hence, the porous film on the top of the TNA plays a role as the protecting layer from dissolution, and consequently the preparation of long nanotubes is possible.

The side walls of the TNAs have obvious thickness variation, which often refers to ripples, as shown in **Figure 9d**. So far, the ripples are formed due to the periodic oscillations of the current in anodization [12]. Indeed, the bamboo-shaped nanotube, a nanostructure with more drastic ripples along the side walls, has been successfully fabricated by using anodic oxidation with ac voltage [12, 15]. **Figure 9e** shows bamboo-shaped tubes which were synthesized in EG electrolytes containing 0.3 wt % NH_4F and 5 vol % H_2O under different anodization sequences of 60 V for 2 min and 10 V for 2 min. The inset illustrates the anodization sequence for the formation of bamboo-type TNAs. The anodic oxidation growth of bamboo-type TiO_2 nanotubes is illustrated by the schematic in **Figure 9e**, where ridge formation between the second section and third section of nanotubes is at the third high-voltage step [12]. The formation mechanism is that the low-voltage step reduces pH and ion diffusion gradient inside TiO_2 nanotubes and induces formation of bamboo ridges on outer tube walls when a second high-voltage step is conducted [12]. Length and ridge spacing of bamboo-type nanotubes can be easily tuned by adjusting electrolyte composition and time of high-voltage step [12].

Figure 9(g) and **(h)** presents the morphology of a lotus root-shaped nanostructure, which was obtained using anodizing voltage of 30 V in the second step and 60 V in the first step. The nanostructure exhibits two levels, and it resembles as a lotus root in shape. The first level consists of cells with size of approximately 0.2 μm, as highlighted by a hexagon in the inset of **Figure 9g** [15]. The second-level structure is constituted by the pores with smaller diameters inside the cells (one of them highlighted by a circle in the inset of **Figure 9g**). Noticeably, the nanopores all evolved in the interior of the cells or such nanopores did not extend across any neighboring cells. By comparing the size and shape, it is found that the first-level structure corresponds to the imprints of Ti surface after the removal of the nanotube layer in the one-step anodization. In addition, this lotus root-shaped nanostructure was only obtained when the second-step voltage was low enough [15]. When the second-step voltage is lower than the first-step voltage, for example, 30 vs. 60 V, the generated nanotubes in the second-step anodization will be thinner than those generated in the first-step anodization. Therefore, several nanotubes simultaneously developed inside one imprint to result in the lotus root-shaped nanostructure, as shown in **Figure 9(g)** and **(h)** [15].

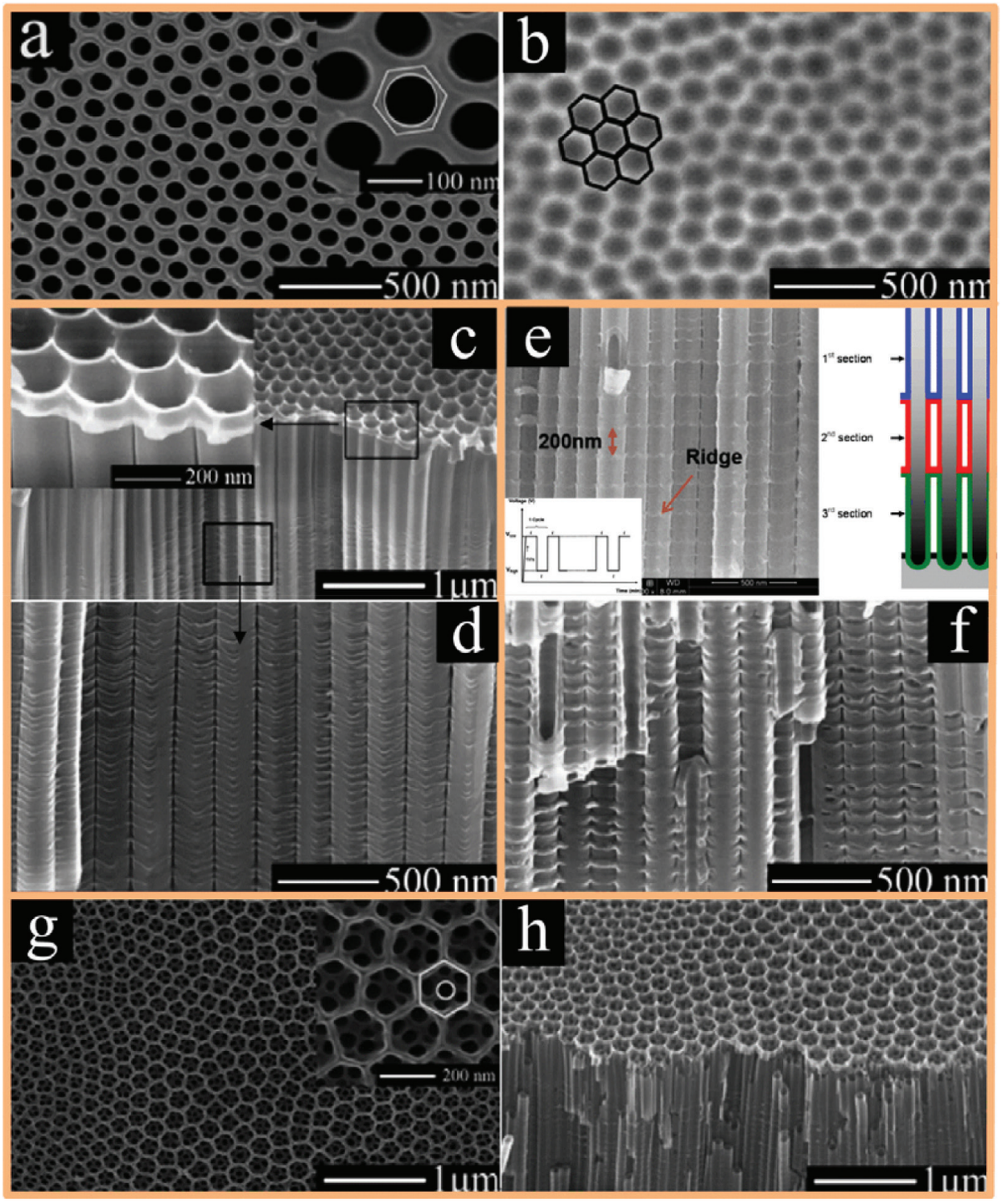

Figure 9. Nanotube array generated in the two-step anodization under a 60 V voltage: (a) top view and (b) the exposed Ti surface after the removal of the nanotube layer. Side view of the TiO_2 nanotubes generated in the two-step anodization: (c) the side view of the nanotubes and (d) zoom-in view of the nanotubes with the ripple features [15]. (c) the bamboo-shaped tubes were synthesized in EG electrolytes containing 0.3 wt % NH_4F and 5 vol % H_2O under different anodization sequences of 60 V for 2 min and 10 V for 2 min. (inset) Anodization sequence for the formation of bamboo-type TiO_2 nanotube arrays. Schematic showing growth of bamboo-type TiO_2 nanotubes via anodic oxidation: Ridge formation between the second section and third section of nanotubes at the third high-voltage step [12]. (f) the bamboo-shaped tubes generated under another square-waved anodizing voltage (the 30 V voltage lasted 90 s and the 60 V voltage still lasted 10 s). (g) and (h) Lotus root-shaped nanostructure obtained under a 30 V anodizing voltage in the two-step anodization: (a) top view and (b) side view [15].

http://dx.doi.org/10.5772/intechopen.77063

3.2. Modified TNAs designed by two-step anodic oxidation

Figure 10(a) presents the two-step anodization process and morphological characteristics under three different voltage regimes of the one-step anodization. Fascinating hierarchical top layer/TNAs has been successfully fabricated by using two-step anodization with controlled anodizing voltages [6]. The electrolytes consisted of 0.5 wt% NH_4F in EG solution with 2 vol% water. The one-step anodization was conducted at anodizing voltages of 60, 80, or 100 V for 60 min to grow TNAs on Ti sheet, and then the as-grown TNAs were ultrasonically removed in DI water. The Ti sheet surface has a regular hexagonally packed round concave morphology (see **Figure 10a**). Next, the second-step anodization was performed using the same Ti sheet at various potentials of 20–100 V and tunable processing time to control the thickness of TNAs. Finally, samples were cleaned with DI water, dried with nitrogen gas, and annealed at 450°C for 1 h in the air.

The hierarchical top layer/TNAs are an outcome of the competition between the electric field-driven anodic oxidation [reaction (1) above, $v_{electro}$] of Ti to form TiO_2 and the electric field-assisted chemical dissolution of the TiO_2 layer [reaction (3) above, v_{dis}] [8, 14]. The anodic oxidation reaction occurs as Ti^{4+} ejection and deposition on the surface in the form of TiO_2, while the TiF_6^{2-} etching reaction occurs from the top to bottom of the as-grown TiO_2. The anodic oxidation rate is very fast and dominated over the NH_4F etching rate, resulting in a thin oxide layer in the early stage [14, 15]. In the late stage, the deposition rate of TiO_2 at the entrance of the nanotubes slows down, while field-induced random dissolution of the surface becomes more significant or dominant to form pore-like structures, which further develop into TNA structures [8, 14]. At certain relative rates between TiO_2 deposition and

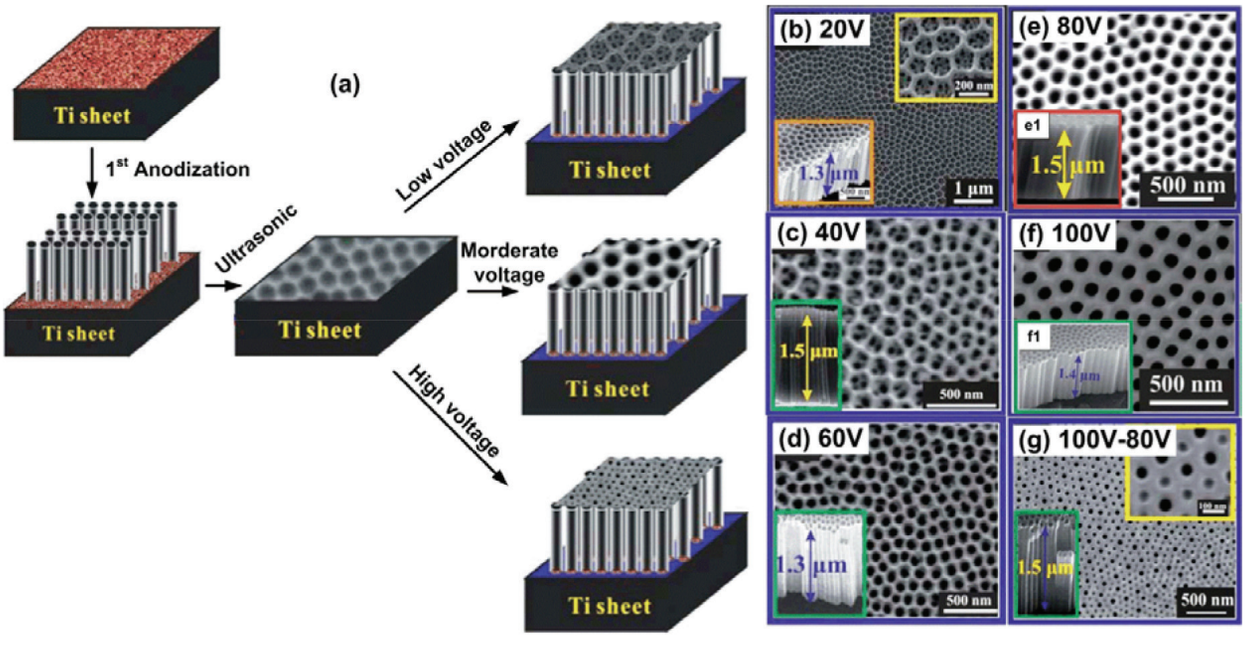

Figure 10. (a) Two-step anodization synthesis of the hierarchical TiO_2 nanotubes. (b–f) Plan-view and cross-sectional scanning electron microscopy (SEM) images of the hierarchical TiO_2 nanotubes prepared at a fixed one-step voltage of 60 V and various two-step voltages from 20 to 100 V. (g) the TNAs prepared at 100 V for the first step and 80 V for the second step [6].

dissolution, a layer of interconnected nanopores can be constructed on the top of TiO_2, as shown in **Figure 10** [6]. The highly ordered hexagonal imprints after ultrasonication plays as a template for the subsequent growth of TNAs with a hierarchical porous top layer [15].

Figure 10(b)–(f) shows SEM images of the modified TNAs prepared at a fixed voltage of 60 V for the one-step anodization and at different voltages from 20 to 100 V for the two-step anodization. **Figure 10(g)** is the TNAs prepared at 100 V for the first step and 80 V for the second step. When the density of applied electric field increases, $v_{electro}$ increases, whereas v_{dis} decreases due to Coulomb force on the TiF_6^{2-} anion. Thus, the unique nanoring/nanotube hierarchical nanostructures is formed at the low two-step voltages of 20 and 40 V because of the relatively high v_{dis}, relatively little accumulation/deposition of $Ti(OH)_4$ occurred at the openings of the nanotubes where the nanotubes met the bulk electrolyte (**Figure 10(b)–(c)**). As the anodization voltage increases further, the accumulation/deposition of $Ti(OH)_4$ at the entrance of the nanotubes increases to form nanopore and nanohole top structures, with the diameters of the openings decreasing with increasing voltages. Furthermore, at high anodization voltages, an increase in $v_{electro}$ favors the formation of a thicker oxide layer owing to the preferred growth at the bottom of the concavity generated in the one-step anodization where the electrical resistance is the lowest. Consequently, the diameters of the bottom tubes of TNAs increase with increasing voltages (**Figure 10(d)–(f)**) [6]. To investigate the effect of the voltage in the one-step anodization step, a comparison between **Figure 10e** (S-60-80) and **10 g** (S-100-80) can be made. Clearly, S-60-80 exhibits a nanopore/TNA structure, whereas S-100-80 presents a nanohole-nanocave/TNA structure, which consists of holes with a pore size of ~50 nm and concaves with closed bottoms. The formation of a thick oxide barrier layer in the one-step anodization step at the high voltage (i.e., 100 V) should be attributed to the formation of S-100-80 morphology. The insets in **Figure 10** confirm that all samples had a uniform length of TNAs in the range of 1.3–1.5 μm for minimizing the effect of tube length disparity on PEC performance.

The photocurrent densities of different samples were determined by linear sweep photovoltammetry measurements using a three-electrode electrochemical system in a 1 M KOH electrolyte under AM 1.5 G (100 mW/cm^2) illumination. Three major conclusions can be drawn from the results in **Figure 11(a)**. (1) The photocurrent densities of all samples prepared by two-step anodization are consistently higher than the ones prepared by the conventional one-step method under the same conditions. This implies that the hierarchical TiO_2 nanostructures favor better PEC performances. Indeed, the one-step prepared TNAs only obtained a photocurrent density of 0.345 $mAcm^{-2}$ at 0.23 V vs. Ag/AgCl or 1.23 V vs. RHE, which is the potential often chosen as a metric to evaluate the performance of photoanodes as it corresponds to the water oxidation potential. Among all samples, S-60-80 achieved the highest photocurrent density of 1.59 $mAcm^{-2}$ at the same potential [6]. (2) The photocurrent densities (I) of different nanostructured TNAs presented a general order of $I_{nanopore/TNA} > I_{nanoring/TNA} > I_{nanohole\text{-}nanocave/TNA}$. The photocurrent density of the nanohole-nanocave/TNA sample (i.e., S-100-80) possesses a low value of 0.480 $mAcm^{-2}$ that should be due to the closed nanocave structures on its surface, and thus it effectively blocks the light absorption and solution infiltration. Moreover, the nanopore/TNA samples (i.e., S-60-60, S-60-80, and S-60-100) exhibited higher photocurrent densities than the nanoring/TNA samples (i.e., S-60-20 and

http://dx.doi.org/10.5772/intechopen.77063

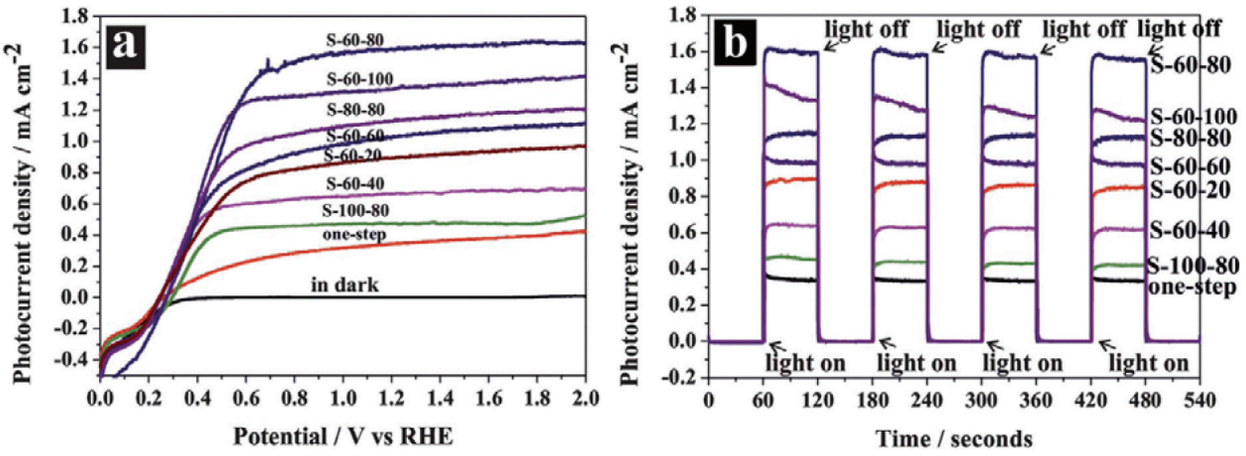

Figure 11. Photoelectrochemical properties of hierarchical TiO_2 nanotube electrodes: (a) linear-sweep voltammograms collected with a scan rate of 5 mVs^{-1} In the dark and under illumination and (b) amperometric *I–t* curves at an applied potential of 1.23 V vs. RHE under illumination with 60 s light on/off cycles [6].

S-60-40) because the formers have better degree of crystallinity and higher optical absorption (to be discussed in the later section). (3) Among all of the nanopore/TNA samples, S-60-80 achieved the highest photocurrent density, which attributed to its better optical absorption and its uniform morphology for reducing structural defects that serve as photoelectron/hole recombination centers (**Figure 10e**) and thus favor high PEC performance.

A photocatalyst material with a better optical absorption and higher crystallinity will subsequently result in a better PEC performance. *P. Wang* et al. found that all two-step hierarchical TNA samples exhibited better UV–Vis absorption than one-step TNA sample because of their unique hierarchical nanostructures and improved morphological uniformity [6]. A better surface morphological uniformity should result in enhanced optical absorption because the material has better periodicity of the photonic crystals formed by the top porous layers. It is found that the crystallite size of TNAs increases with increasing anodizing voltages [22]. Therefore, a high anodizing voltage favors the formation of bigger crystal nucleus and thus results in a better crystallinity and less defects to obtain the better PEC performance, which agreed well with the aforementioned results [6]. In addition, the photoelectrode stability of the hierarchical TNAs was assessed via amperometric (I − t) measurements, performing at a fixed electrode potential of 1.23 V vs. RHE under alternating light on and light off with a cycle of 60 s. As can be seen in **Figure 11(b)**, fast photoresponses were recorded for all samples, and this photocurrent pattern was highly reproducible for many on/off cycles [6].

4. Conclusions

It is demonstrated that various spectacular and interesting 1D nanostructures of TiO_2 have been grown and designed by anodic oxidation. TiO_2 nanotube arrays and TiO_2 nanowires/nanotubes are generally obtained by conventional one-step anodic oxidation with suitable conditions. The effects of anodizing voltage, processing time, and electrolytes on the morphologies of anodic oxidation TiO_2 nanomaterials are reported. Meanwhile, two-step anodic

oxidation allows growing some spectacular TiO_2 nanostructures such as highly ordered TNAs, bamboo-type TNAs, and lotus root-shaped TNAs. In addition, the formation mechanisms and photocatalytic activities of some TNA-based nanomaterials prepared by anodic oxidation are presented and discussed.

Acknowledgements

Financial support from the Vietnam National Foundation for Science and Technology Development (NAFOSTED) under grant number 103.99-2016.75 (P.H. Le) and the Ministry of Science and Technology, Taiwan, under grant number, 106-2221-E-009-157 (J. Leu), is gratefully acknowledged.

Author details

Phuoc Huu Le[1]* and Jihperng Leu[2]*

*Address all correspondence to: lhuuphuoc@ctump.edu.vn and jimleu@mail.nctu.edu.tw

1 Faculty of Basic Sciences, Can Tho University of Medicine and Pharmacy, Can Tho, Vietnam

2 Department of Materials Science and Engineering, National Chiao Tung University, Hsinchu, Taiwan

References

[1] Roy P, Berger S, Schmuki P. TiO_2 nanotubes: Synthesis and applications. Angewandte Chemie International Edition. 2011;**50**:2904-2939. DOI: 10.1002/anie.201001374

[2] Mohamed AER, Rohani S. Modified TiO_2 nanotube arrays (TNTAs): Progressive strategies towards visible light responsive photoanode—A review. Energy & Environmental Science. 2011;**4**:1065. DOI: 10.1039/c0ee00488j

[3] Lai CW, Juan JC, Ko WB, Bee S, Hamid SBA. An overview: Recent development of titanium oxide nanotubes as photocatalyst for dye degradation. International Journal of Photoenergy. 2014;**2014**:524135. DOI: 10.1155/2014/524135

[4] Yin ZF, Wu L, Yang HG, Su YH. Recent progress in biomedical applications of titanium dioxide. Physical Chemistry Chemical Physics. 2013;**15**:4844-4858. DOI: 10.1039/c3cp43938k

[5] Kubacka A, Fernández-García M, Colón G. Advanced nanoarchitectures for solar photocatalytic applications. Chemical Reviews. 2012;**112**:1555-1614. DOI: 10.1021/cr100454n

[6] Zhang Z, Wang P. Optimization of photoelectrochemical water splitting performance on hierarchical TiO_2 nanotube arrays. Energy & Environmental Science. 2012;**5**:6506. DOI: 10.1039/c2ee03461a

[7] Hoffmann MR, Martin ST, Choi W, Bahnemann DW. Environmental applications of semiconductor photocatalysis. Chemical Reviews. 1995;**95**:69-96

[8] Yan J, Zhou F. TiO_2 nanotubes: Structure optimization for solar cells. Journal of Materials Chemistry. 2011;**21**:9406. DOI: 10.1039/c1jm10274e

[9] Reyes-Coronado D, Rodriguez-Gattorno D, Espinosa-Pesqueira ME, Cabb C, De Cross R, Oskam G. Phase-pure TiO_2 nanoparticles: Anatase, brookite and rutile. Nanotechnology. 2008;**19**:145605. DOI: 10.1088/0957-4484/19/14/145605

[10] Hsu M-Y, Hsu H-L, Leu J. TiO_2 nanowires on anodic TiO_2 nanotube arrays (TNWs/TNAs): Formation mechanism and photocatalytic performance. Journal of the Electrochemical Society. 2012;**159**:H722-H727

[11] Turkevych I, Pihosh Y, Hara K, Wang Z-S, Kondo M. Hierarchically organized micro/nano-structures of TiO_2. Japanese Journal of Applied Physics. 2009;**48**:06FE02. DOI: 10.1143/JJAP.48.06FE02

[12] Luan X, Guan D, Wang Y. Facile synthesis and morphology control of bamboo-type TiO_2 Nanotube arrays for high-efficiency dye-sensitized solar cells. The Journal of Physical Chemistry C 2012;**116**:14257−14263. DOI: 10.1021/jp305280q

[13] Ge MZ, Cao C-Y, Huang J-Y, Li S-H, Zhang S-N, Deng S, Li Q-S, Zhang K-Q, Lai YK. Synthesis, modification, and photo/photoelectrocatalytic degradation applications of TiO_2 nanotube arrays: A review. Nanotechnology Reviews. 2016;**5**:75-112. DOI: 10.1515/ntrev-2015-0049

[14] Wang D, Yu B, Wang C, Zhou F, Liu W. A novel protocol toward perfect alignment of anodized TiO_2 nanotubes. Advanced Materials. 2009;**21**:1964-1967. DOI: 10.1002/adma.200801996

[15] Li S, Zhang G, Guo D, Yu L, Zhang W. Anodization fabrication of highly ordered TiO_2 nanotubes. Journal of Physical Chemistry C. 2009;**113**:12759-12765. DOI: 10.1021/jp903037f

[16] Zwilling V, Darque-Ceretti E, Boutry-Forveille A, David D, Perrin MY, Aucouturier M. Structure and physicochemistry of anodic oxide films on titanium and TA6V alloy. Surface and Interface Analysis. 1999;**27**:629

[17] Nie X, Chen J, Li G, Shi H, Zhao H, Wong PK, An T. Synthesis and characterization of TiO_2 nanotube photoanode and its application in photoelectrocatalytic degradation of model environmental pharmaceuticals. Journal of Chemical Technology and Biotechnology. 2013;**88**:1488-1497. DOI: 10.1002/jctb.3992

[18] Pichat P, Disdier J, Hoang-Van C, Mas D, Goutailler G, Gaysse C. Purification/deodorization of indoor air and gaseous effluents by TiO_2 photocatalysis. Catalysis Today. 2000;**63**:363-369

[19] Lim JH, Choi J. Titanium oxide nanowires originating from anodically grown nanotubes: The bamboo-splitting model. Small. 2007;**3**:1504-1507. DOI: 10.1002/smll.200700114

[20] Sharma SD, Saini KK, Kant C, Sharma CP, Jain SC. Photodegradation of dye pollutant under UV light by nano-catalyst doped titania thin films. Applied Catalysis B: Environmental. 2008;**84**:233-240. DOI: 10.1016/j.apcatb.2008.04.017

[21] Ye M, Xin X, Lin C, Lin Z. High efficiency dye-sensitized solar cells based on hierarchically. Nano Letters. 2011;**11**:3214-3220. DOI: 10.1021/nl2014845

[22] Allam NK, Grimes CA. Room temperature one-step polyol synthesis of anatase TiO_2 nanotube arrays: Photoelectrochemical properties. Langmuir. 2009;**25**:7234-7240. DOI: 10.1021/la9012747